

Application of explicit FE codes to simulation of sheet and bulk metal forming processes

J. Rojek ^{a,*}, E. Oñate ^b, E. Postek ^a

^a Institute of Fundamental Technological Research, Polish Academy of Sciences, ul. Swietokrzyska 21 PL-00049 Warsaw, Poland

^b International Center for Numerical Methods in Engineering, Barcelona, Spain

Abstract

This paper presents the application of an explicit dynamic finite element code for simulation of metal forming processes, of both sheet and bulk forming. The experiences reported here have been gained during the development and use of our own explicit program Stampack. An original formulation of a triangular shell element without rotational degrees of freedom is reviewed combining the explicit sheet forming simulation with the implicit springback analysis as well as the parallelization of the explicit program described. An extension of a finite element code for coupled thermomechanical analysis is discussed. A new thermomechanical constitutive model developed by the authors and implemented in the program is presented. Numerical examples illustrate some of the possibilities of the finite element code developed. © 1998 Elsevier Science S.A. All rights reserved.

Keywords: Metal forming; Sheet stamping; Finite element simulation; Explicit dynamic analysis; Thermomechanical analysis

1. Introduction

Finite element programs based on the explicit dynamic formulation have proved to be a very attractive tool for the simulation of metal forming processes. Explicit time integration schemes deal with the system of discretized equations of motion in the following form:

$$\mathbf{M}\ddot{\mathbf{r}} + \mathbf{D}\dot{\mathbf{r}} = \mathbf{f} - \mathbf{p} \quad (1)$$

where \mathbf{M} and \mathbf{D} are the mass and damping matrices, \mathbf{r} is the nodal displacement vector, and \mathbf{f} and \mathbf{p} are the vectors of external and internal nodal forces, respectively. Employing Eq. (1) for the known configuration at time t_n the solution for the next time instant $t_{n+1} = t_n + \Delta t$ is obtained. The effectiveness of the explicit formulation is based on the use of a diagonal mass matrix. There are also disadvantages, the main one is the limitation of the time step due to the conditional stability. The numerical efficiency, however, and other advantages of explicit programs such as low memory requirements and easy treatment of contact conditions, cause this approach to dominate over implicit methods in industrial applications.

The computation times, however, in case of large industrial problems are still quite long. The implementation of a new triangular shell element as well as the use of techniques of parallel computation reduced simulation times considerably.

The explicit program for the simulation of forming has been combined with an implicit solver to perform the analysis of elastic springback efficiently.

The use of explicit finite element programs in the analysis of sheet metal forming has become quite common, while the possibilities of this approach in the simulation of bulk forming seem to be not exploited sufficiently as yet. These problems require taking account of the thermal effects in the deformation process that can be achieved by the coupled thermo-mechanical analysis.

2. Simple and efficient finite element formulation for sheet stamping simulation

Efficiency is a very important factor in industrial applications of finite element simulation. It depends considerably on the finite element formulation used. Efficient solutions can be usually achieved by using elements based on simple theoretical assumptions.

* Corresponding author.

Simplicity of the formulation must not be obtained, however, at the cost of loss of its precision. The simplicity of the element developed for the simulation of sheet stamping and implemented in our code is based on avoiding the use of rotational degrees of freedom which yields a triangular shell element with three degrees of freedom per node only.

The work on the element with translational degrees of freedom only, the so-called BST (Basic Shell Triangle) element has been started by Oñate and Cervera [1] and continued by Oñate and Zarate [2]. The element formulation for an explicit dynamic program has been presented in [3,4].

The shell deformation is described in terms of the deformation of its midsurface. With the assumption of the Kirchhoff hypothesis the rate of deformation tensor at any point of the shell $\dot{\epsilon} = \{\dot{\epsilon}_x, \dot{\epsilon}_y, \dot{\epsilon}_z\}^T$ can be written in the following way:

$$\dot{\epsilon} = \dot{\epsilon} + z\dot{\kappa} \tag{2}$$

where z is the distance of the current material point to the midsurface, $\dot{\epsilon} = \{\dot{\epsilon}_{xx}, \dot{\epsilon}_{yy}, \dot{\epsilon}_{xy}\}^T$ and $\dot{\kappa} = \{\dot{\kappa}_{xx}, \dot{\kappa}_{yy}, \dot{\kappa}_{xy}\}^T$ are the rates of membrane and bending deformation of the midsurface, respectively.

The BST element employs linear shape functions so the membrane component of the element is equivalent to the standard constant strain triangle (CST) element. The bending part is formulated using a finite-volume-like procedure presented in [1] which allows expression of the rate of bending deformation $\dot{\kappa}$ within an element in terms of the gradient of deflection velocity w along the element sides:

$$\dot{\kappa} = \frac{1}{A} \int_{\Gamma} \mathbf{Q} \nabla w \, d\Gamma \tag{3}$$

where

$$\mathbf{Q} = \begin{bmatrix} n_x & 0 \\ 0 & n_y \\ n_y & n_x \end{bmatrix} \quad \nabla = \left\{ \frac{\partial}{\partial x}, \frac{\partial}{\partial y} \right\}^T \tag{4}$$

with A being an area of the element, Γ its contour, x and y are the local Cartesian coordinates, and $\mathbf{n} = \{n_x, n_y\}^T$ is a unit vector normal to the boundary defined in the plane of the element (Fig. 1). The deflection gradient along the element sides is in turn calculated in terms of the nodal velocities of the adjacent elements shown in Fig. 1.

The elasto-plastic model adopted for the BST element assumes a hypoelastic rate constitutive law

$$\overset{\nabla}{\boldsymbol{\sigma}} = \mathbf{C}^{ep} \mathbf{d} \tag{5}$$

where $\overset{\nabla}{\boldsymbol{\sigma}}$ is the Jaumann rate of the Cauchy stress tensor and \mathbf{C}^{ep} is the elasto-plastic constitutive tensor. Yielding is considered using the anisotropic Hill (1979) yield criterion [5].

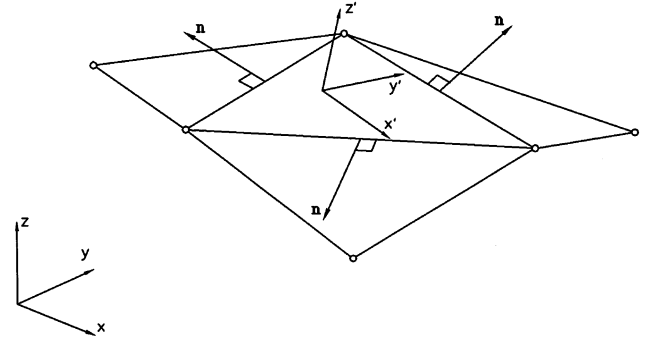


Fig. 1. Finite element patch.

The BST element has been successfully applied to sheet forming analysis with an explicit dynamic program, [6]. A number of large industrial problems have been analysed yielding good results.

3. Springback simulation

The dynamic analysis of forming can be extended to the springback phase—once the final deformation is obtained, the simulation can be continued with contact conditions removed and adequate damping to obtain a steady state solution that will yield the deformed shape after springback. Experience, however, shows that this approach is very inefficient since the time required for the springback analysis is very long and usually exceeds the time of the simulation of forming. The reason is that the critical time step is very small compared with the period of natural vibrations.

The springback problem can be solved efficiently by combining the explicit simulation of forming with implicit analysis of the springback. Both implicit dynamic and quasistatic schemes are possible. The implicit dynamic solution schemes are obtained by taking equations of motion (Eq. (1)) for the unknown configuration at time t_{n+1} denoted by the subscript $n + 1$ to get the solution for this configuration

$$\mathbf{M}\ddot{\mathbf{r}}_{n+1} \mathbf{D}\dot{\mathbf{r}}_{n+1} = \mathbf{f}_{n+1} - \mathbf{p}_{n+1} \tag{6}$$

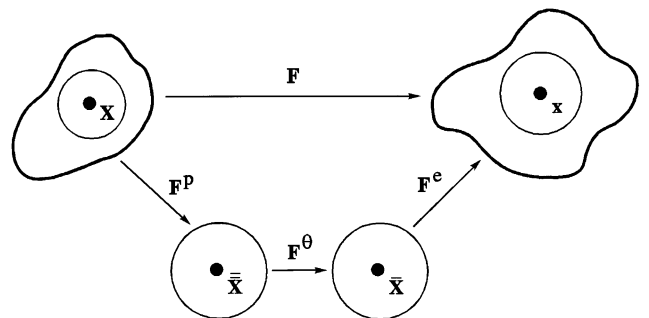


Fig. 2. Multiplicative decomposition of the deformation gradient tensor.

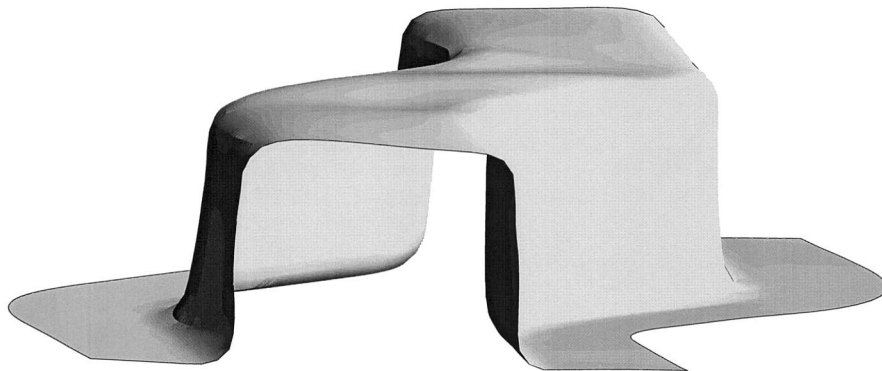


Fig. 3. Deformed shape after springback.

The right-hand side of Eq. (6) depends on the solution looked for, i.e.

$$p_{n+1} = p_{n+1}(r_{n+1}, \sigma_{n+1}) \quad (7)$$

so the solution to the problem expressed by Eq. (6) can be obtained by an iterative procedure. Similarly, a quasistatic implicit problem

$$f_{n+1} - p_{n+1} = 0 \quad (8)$$

can be solved iteratively.

In the springback analysis there is no external loading, thus $f=0$. The residual force appear due to the residual stresses in the sheet at the end of forming. The implicit module for our explicit program has been developed and a number of problems, including industrial ones, have been analysed. In some cases it was possible to perform an implicit springback analysis at one step. In the case of large springback effects, however, it was necessary to use more steps applying the residual stresses incrementally. One of the examples analysed is presented in this paper.

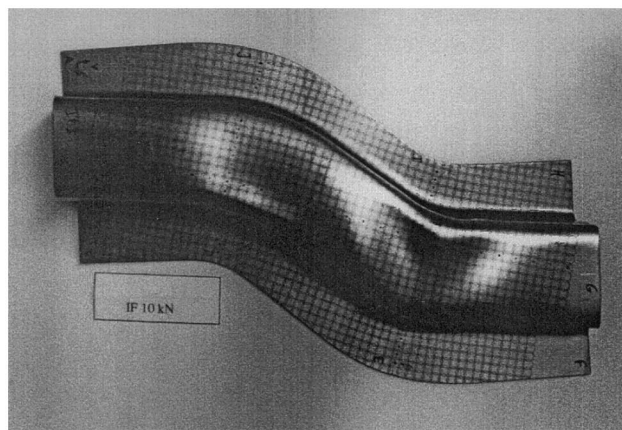
4. Parallel processing

Parallel processing offers another possibility to reduce real time of the sheet stamping simulation. Explicit dynamic programs are suitable for parallelisation. During the explicit stamping computations $\sim 80\text{--}90\%$ of the CPU time is used at the elemental level in the calculation of strains, stresses and internal nodal forces. The rest of the CPU time is used mainly in the contact and time integration routines. The fact that most of the calculation are performed at the elemental level means that great speed-ups can be expected using the technique of parallel computing. Therefore our explicit software has been parallelised recently [7].

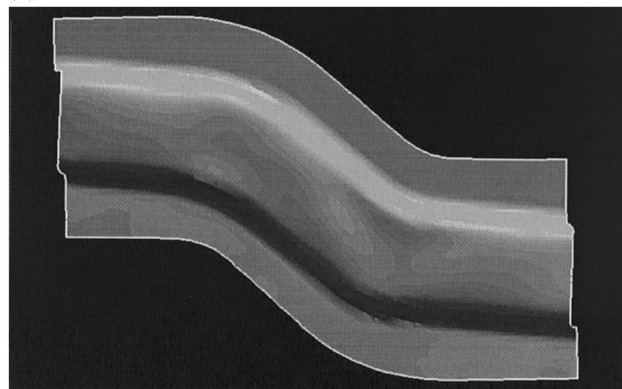
The approach used follows a distributed memory procedure in which the geometry is divided into a number of domains, usually equal to the number of processors available. Each processor is then responsible

for all the computations related to its own domain, inter-communicating with the other domains when passing the information about elements or nodes along the common boundaries is required.

The software has been targeted to run on networks of PCs (under Windows NT) or networks of workstations (under Unix), but shared memory machines can also be used. The effectiveness of the parallel version of Stampack has been confirmed in the simulation of practical sheet stamping problems.



(a)



(b)

Fig. 4. Comparison of deformed shapes obtained in experiment and simulation.

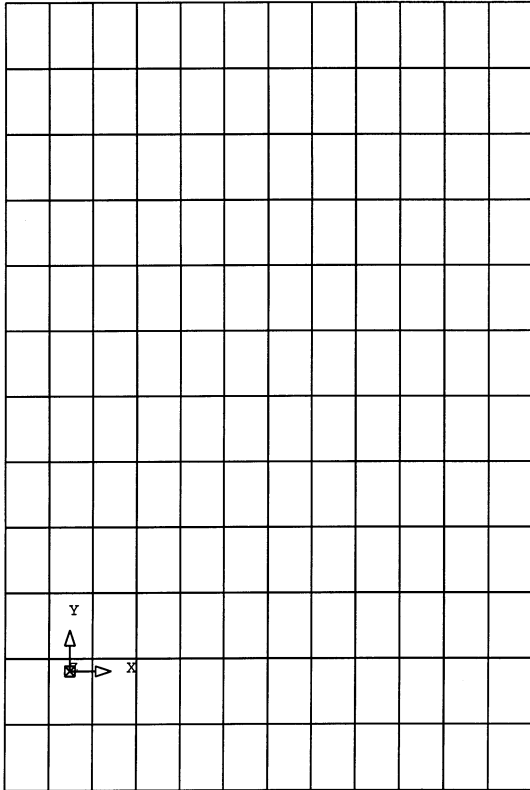


Fig. 5. Finite element discretization of the billet.

5. Explicit thermomechanical analysis

Simulation of bulk forming processes requires taking into account the thermal effects and interactions of thermal and mechanical phenomena. The algorithm for a coupled thermomechanical analysis has been implemented in our explicit program making it possible to analyse such forming processes.

In the solution of a thermomechanical problem the solution of the mechanical problem (Eq. (1)) is coupled with the solution of the heat conduction problem governed by the following discretized equation:

$$C\dot{T} + \mathbf{K}T = \mathbf{Q} \tag{9}$$

where \mathbf{C} is the heat capacity matrix, \mathbf{K} is the heat conductivity matrix, \mathbf{Q} is the heat flux and sources vector, and T is the vector of nodal temperatures. Eqs. (1) and (9) are solved under adequate boundary conditions. Eq. (9) can be solved using either an explicit or implicit scheme of time integration. At present the forward Euler explicit time integration method has been implemented for the solution of Eq. (9) in the numerical algorithm for the thermomechanical analysis. This combined with the central difference time integration of Eq. (1) gives the following fully explicit scheme for a coupled problem:

$$\ddot{r}_n = \mathbf{M}_D^{-1}(\mathbf{f}_n - \mathbf{p}_n - \mathbf{D}\dot{r}_n), \quad \mathbf{M}_D = \text{diag } \mathbf{M} \tag{10}$$

$$\dot{r}_{n+1/2} = \dot{r}_{n-1/2} + \ddot{r}_n \Delta t \tag{11}$$

$$r_{n+1} = r_n + \dot{r}_{n+1/2} \Delta t \tag{12}$$

$$T_{n+1} = \mathbf{C}_D^{-1}(\mathbf{Q}_n - \mathbf{K}_n T_n), \quad \mathbf{C}_D = \text{diag } \mathbf{C} \tag{13}$$

The new configuration r_{n+1} is obtained from the explicit equations of motion with the temperatures assumed fixed, and the new temperature T_{n+1} is calculated at constant geometry. The results are exchanged at each step and coupling term are calculated. Eqs. (1) and (9) for the thermo-mechanical problem are coupled by considering the following effects:

- heat generation by the plastic dissipation,
- contribution of the thermal expansion to the total material deformation,
- influence of the temperature on the yield stress of the material.

The rate of heat generation q due to the plastic dissipation (contributing to the vector \mathbf{Q}) can be calculated as:

$$q = \chi \sigma : d^p \tag{14}$$

where: σ is the Cauchy stress tensor, d^p is the rate of plastic deformation tensor, and χ is the fraction of plastic work converted to heat. The method of accounting for the thermal effects in the constitutive model developed is presented in the next section.

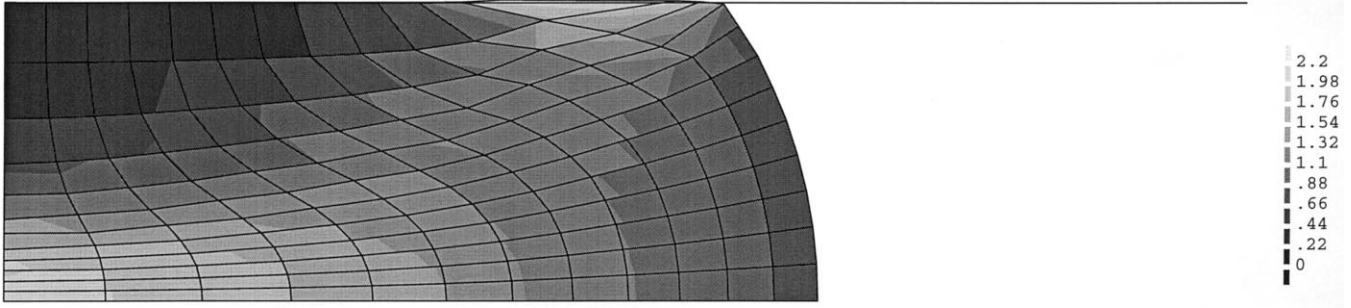


Fig. 6. Deformed shape at 60% upsetting with the plastic strain distribution (thermal softening not considered).

6. Thermo-elastoplastic constitutive model

A new thermo-elastoplastic model has been developed and implemented in the explicit dynamic code Stampack. The model employs the concept of hyperelasticity. The main advantage of hyperelastic models compared with hypoelastic formulations is the absence of need for calculation of derivatives satisfying the criteria of objectivity and of a need for integration of the constitutive equations [8,9].

Formulation of the constitutive model for the thermo-elastoplastic material is an extension of that of the elastoplastic model presented in [9,10] to the thermo-elastoplastic problems. In the description of large thermo-elastoplastic deformations we assume multiplicative decomposition (see Fig. 2) of the deformation gradient tensor \mathbf{F} into its elastic, thermal and plastic parts, \mathbf{F}^e , \mathbf{F}^θ and \mathbf{F}^p , respectively:

$$\mathbf{F} = \mathbf{F}^e \mathbf{F}^\theta \mathbf{F}^p \quad (15)$$

with

$$\det \mathbf{F}^p = 1, \quad (16)$$

$$\mathbf{F}^\theta = J_\theta \mathbf{I}, \quad \text{where} \quad J_\theta = e^{3\alpha(T - T_0)} \quad (17)$$

The Almansi strain tensor \mathbf{e} can be expressed by means of the deformation gradient tensor \mathbf{F} as

$$\mathbf{e} = \frac{1}{2}(\mathbf{I} - \mathbf{F}^{-T} \mathbf{F}^{-1}) \quad (18)$$

Analogically to Eq. (18) we define the elastic Almansi tensor \mathbf{e}^e (in the spatial configuration) and the thermal Almansi tensor $\bar{\mathbf{e}}^\theta$ (in the intermediate configuration):

$$\mathbf{e}^e = \frac{1}{2}(\mathbf{I} - \mathbf{F}^{e-T} \mathbf{F}^{e-1}) \quad (19)$$

$$\bar{\mathbf{e}}^\theta = \frac{1}{2}(\mathbf{I} - \mathbf{F}^{\theta-T} \mathbf{F}^{\theta-1}) \quad (20)$$

After transforming the thermal Almansi tensor to the spatial configurations (the push-forward operation):

$$\mathbf{e}^\theta = \frac{1}{2} \mathbf{F}^{e-T} (\mathbf{I} - \mathbf{F}^{\theta-T} \mathbf{F}^{\theta-1}) \mathbf{F}^{e-1} \quad (21)$$

we can introduce the following additive relation:

$$\mathbf{e} = \mathbf{e}^e + \mathbf{e}^\theta + \mathbf{e}^p \quad (22)$$

defining the plastic Almansi tensor \mathbf{e}^p . Applying the Lie derivative L_v to all the components of the Almansi tensor in Eq. (22) we obtain the additive decomposition of the deformation rate tensor

$$\mathbf{d} = \mathbf{d}^e + \mathbf{d}^\theta + \mathbf{d}^p \quad (23)$$

The stress response is characterized by means of the elastic free energy function of the form:

$$\psi^e = \frac{1}{2} \lambda \operatorname{tr}(\mathbf{e}^e)^2 + \mu (\mathbf{e}^e : \mathbf{e}^e) \quad (24)$$

where λ and μ are the Lamé constants. With this form of the elastic potential the constitutive relation obtained for the Cauchy stress follows:

$$\boldsymbol{\sigma} = \frac{\partial \psi(\mathbf{e}^e)}{\partial \mathbf{e}^e} = \lambda \operatorname{tr}(\mathbf{e}^e) \mathbf{1} + 2\mu \mathbf{e}^e \quad (25)$$

The stresses are calculated in a two-step algorithm, the first step is the elastic predictor, and the second one the plastic corrector employing the radial return. For the plastic deformation the associated flow rule is assumed:

$$\mathbf{d}^p = L_v(\mathbf{e}^p) = \dot{\lambda} \frac{\partial f}{\partial \mathbf{e}^p} \quad (26)$$

with the Von Mises yield condition:

$$f = \sqrt{\frac{3}{2}} - \sigma_Y(\bar{\mathbf{e}}^p, T) \leq 0 \quad (27)$$

that accounts for the isotropic hardening and thermal softening:

$$\sigma_Y = [\sigma_0 = (\sigma_\infty - \sigma_0)(1 - e^{-\delta \bar{\mathbf{e}}^p}) + H \bar{\mathbf{e}}^p][1 - H_\theta(T - T_0)] \quad (28)$$

where τ —the deviatoric Cauchy stresses, σ_0 and σ_∞ —initial and final yield stress, δ —saturation constant, H —hardening modulus and H_θ —thermal softening modulus.

The form of the elastic potential (Eq. (24)) is based on the assumption that the elastic part of the strains \mathbf{e}^e is small, which is fully justified for metals. It is assumed for reasons of simplicity and efficiency. Some authors starting from the same basic assumption expressed by Eq. (15), [11], have developed more general models, considering the possibility of large elastic deformations. Our formulation is simpler in implementation and no

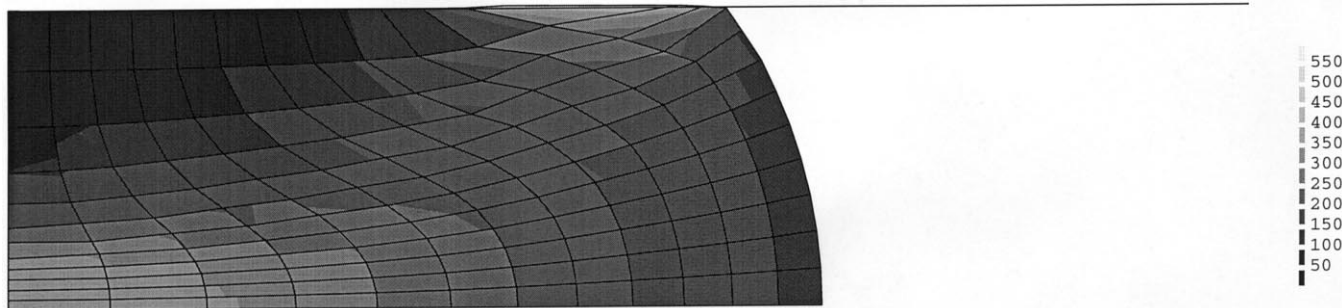


Fig. 7. Deformed shape at 60% upsetting with the temperature distribution (thermal softening not considered).

loss of accuracy in the considered class of problems is expected. Good behaviour of this model in the problems of metal forming without accounting for thermal effects has been confirmed earlier, [10,9,12].

The thermo-elastoplastic model developed has been implemented in the program Stampack for a 4-node element for 2D problems and for a 8-node hexahedral element for 3D analysis. In both elements the mixed formulation (with constant pressure) has been used to avoid element locking. Good results have been obtained for test examples analysed. One of these examples is included in this paper.

7. Numerical examples

7.1. Deep drawing of an S-rail

The deep drawing of an S-rail was one of the benchmark problems defined for the Numisheet '96 conference [13]. This example allows us to validate the correctness and efficiency of our program in a fairly complex example which is well documented, and has been studied experimentally and numerically by many groups. The definition of the benchmark and summary of the results can be found in [13].

Different materials and different blankholding forces have been specified for this example. The solution presented here is for the case of an IF steel and blankholding force of 10 kN. The Young's modulus and Poisson's ratio were $2.06 \cdot 10^5$ and 0.3M Pa, respectively, and transverse anisotropy was considered using

Hill's yield criterion with a Lankford coefficient $R = 1.82$. The stress-strain curve used is given by $\sigma = 526.0(0.0058 + \bar{\epsilon}^p)^{0.233}$ MPa. The friction coefficient for all the sheet-tool interfaces was 0.11. The sheet was discretized with 12000 BST elements.

The first part consisted of the simulation of the stamping process with the required punch stroke of 37 mm. The maximum punch velocity was assumed to be 10 m s^{-1} . The simulation of stamping was carried out in ~ 39000 steps and took ~ 10 h of CPU time on a SG Origin 2000.

After the stamping analysis, both explicit dynamic and implicit quasi-static springback calculations were considered. The springback using the explicit dynamic approach took approximately the same amount of time as the forming simulation, while the springback solution by the quasi-static implicit method took a few minutes only. The shapes obtained in both cases were practically the same. The deformed shape after springback can be seen in Fig. 3, where buckling in the upper part can be observed. The final shape after springback is compared with the shape of a real part in Fig. 4, showing good agreement and accurately predicting buckling of the upper surface. Quantitative comparisons of cross-section profiles between the experimental results and our numerical results demonstrated satisfactory accuracy of our calculations, [13].

The explicit dynamic part of the simulation was run on a network of PCs to evaluate the performance of the parallel version of the software. The serial version of Stampack took 52 h to run the stamping analysis and the time was reduced to 13 h and 30 min, when run on

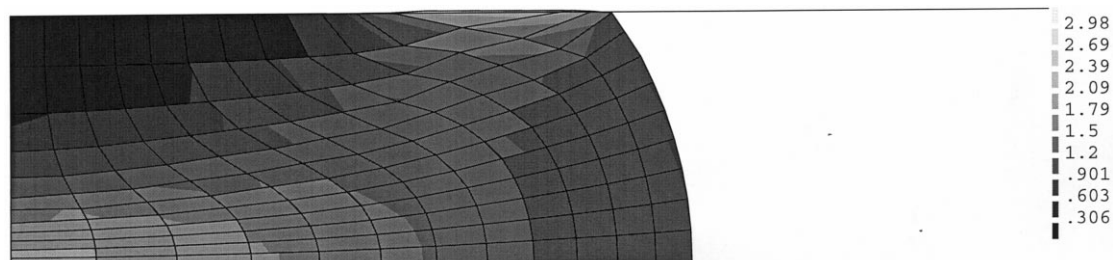


Fig. 8. Deformed shape at 60% upsetting with the plastic strain distribution (with thermal softening).

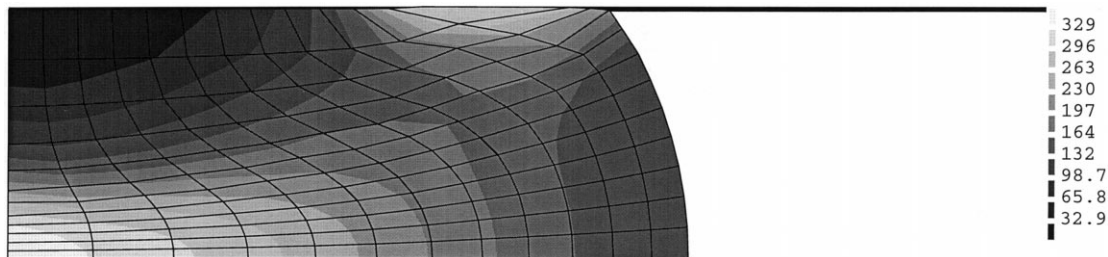


Fig. 9. Deformed shape at 60% upsetting with the temperature distribution (thermal softening).

a network of five PCs; this represents a speed-up factor of 3.8 with an efficiency of 76%.

7.2. Upsetting of a cylindrical billet

This example was used to verify the new thermo-elasto-plastic constitutive model and to test the algorithm of thermo-mechanical analysis implemented in the program Stampack. A cylindrical billet, 30 mm high and with a radius of 10 mm, is compressed between two rigid and rough plates. All the surfaces are assumed to be fully insulated. The problem has been defined originally by Lipmann in [14] and was analysed in [15]. The analysis was carried out to an upset of 60%. The mechanical and thermal properties were: Young's modulus: $E = 2 \cdot 10^5$ MPa, Poisson's coefficient: $\nu = 0.3$, density $\rho = 7833$ kg m^{-3} , yield stress: $\sigma_0 = \sigma_\infty = 700$ MPa, hardening modulus $H = 300$ MPa, thermal softening modulus $H_\theta = 0.002$ $1/^\circ C$, specific heat $c = 586$ J $(kg \cdot ^\circ C)^{-1}$, conductivity $k = 52$ W $(m \cdot ^\circ C)^{-1}$. The material properties were basically the same as those used in [15] except that thermal softening was considered as well. The final deformation was obtained in 0.1 s.

Due to symmetry only a half of the billet was discretized with 144 4-node axisymmetric elements (Fig. 5). Two cases were studied, one without considering the thermal softening (which is reported in [15]) and the other accounting for the thermal softening (which represents better material behaviour in forming).

The results of the analysis for both cases are shown in Figs. 6–9. Figs. 6 and 7 show the plastic strain and temperature distribution for the case without thermal softening.

The maximum values of the plastic strain (2.2) and temperature ($\sim 550^\circ C$) are in perfect agreement with the results obtained with the implicit ABAQUS program [15].

Figs. 8 and 9 present the plastic strain and temperature distribution for the case with thermal softening. The plastic strains in this case are greater and the temperatures lower than in the first case as should be expected. These results and other tests studied confirm the accuracy and correctness of the thermo-mechanical model and algorithm implemented in our explicit dynamic program.

8. Conclusions

The program Stampack was tested on a number of industrial applications of sheet stamping simulation. The formulation of shell element presented in this paper is efficient and gives good results. The program can be considered as a tool suitable for the industrial simulation of sheet forming. New features of the Stampack, the thermo-elastoplastic material model developed and explicit thermo-mechanical algorithm, have been tested. Good results obtained allow us to create a good program for bulk forming as well. Further development of the software, including adaptive remeshing, is planned.

Acknowledgements

The first and third author gratefully acknowledge funding from the Polish Committee for Scientific Research under Grant No. 8T11F01512. The authors also thank J. Duarte from INEGI, Oporto (Portugal) who provided the experimental results of the S-rail benchmark.

References

- [1] E. Oñate, M. Cervera, Derivation of thin plate bending elements with one degree of freedom per node. A simple three node triangle, *Eng. Comput.* 10 (1993) 543–561.
- [2] E. Oñate, F. Zarate, Shell triangles with translational degrees of freedom, Technical report, CIMNE, Barcelona, 1994.
- [3] P. Cendoya, New shell finite elements for elastoplastic dynamic analysis. PhD thesis, Universitat Politècnica de Catalunya, Barcelona, 1996 (in Spanish).
- [4] E. Oñate, P. Cendoya, J. Rojek, J. Miquel, A simple thin shell triangle with translational degrees of freedom only, in: S.N. Atluri, G. Yagawa (Eds.), *Advances in Computational Engineering Science*, Tech Science Press, USA, 1997, pp. 308–313.
- [5] R. Hill, Theoretical plasticity of textured aggregates, *Math. Proc. Cambridge Philos. Soc.* 85 (1979) 179.
- [6] E. Oñate, P. Cendoya, J. Rojek, J. Miquel, A simple thin shell triangle with translational degrees of freedom for sheet stamping analysis, Third International Conference on Numerical Simulation of 3-D Sheet Forming Processes, Numisheet '96, Dearborn, MI, 29 September–3 October, 1996, pp. 102–111.
- [7] G.A. Duffett, L. Neamtu, E. Oñate, J. Rojek, F. Zarate, STAMPAR: a parallel processing approach for the analysis of sheet

- stamping problems. Computational plasticity, Proceedings of the Fifth International Conference, Barcelona, 1997, pp. 1781–1789.
- [8] J.C. Simo, M. Ortiz, A unified approach to finite deformation elastoplastic analysis based on the use of hyperelastic constitutive relations, *Comput. Meth. Appl. Mech. Eng.* 49 (1985) 221–245.
- [9] C. García Garino, J. Oliver, Use of a large strain elastoplastic model for simulation of metal forming processes, in: J.L. Chenot, R. Wood, O.C. Zienkiewicz (Eds.), *NUMIFORM '92*, Balkema, 1992, pp. 467–472.
- [10] C. García Garino, J. Oliver, A numerical model for elastoplastic large strain problems, in: D.R.J. Owen et al. (Eds.), *Computational Plasticity*, 1992, pp. 117–129.
- [11] P. Wriggers, C. Miehe, M. Kleiber, J.C. Simo, On the coupled thermomechanical treatment of necking problems via finite element methods, *Int. J. Num. Meth. Eng.* 33 (1992) 869–883.
- [12] C. García Garino, J. Rojek, E. Oñate, Simulation of sheet metal stamping processes using a solid finite strain model, in: L.A. Godoy, S.R. Idelsohn, P.A.A. Laura, D.T. Mook (Eds.), *Applied Mechanics in the Americas, Proceedings of the Fourth Pan American Congress of Applied Mechanics, PACAM IV*, Santa Fe, Argentina, vol. 1, 1995, pp. 97–102.
- [13] *NUMISHEET '96*, Proceeding of the Third International Conference: Numerical Simulation of the 3-D Sheet Metal Forming Processes, Dearborn, MI, 1996.
- [14] H. Lippmann, *Metal Forming Plasticity*, Springer, Berlin, 1979.
- [15] *ABAQUS, Examples manual*, Version 5.6. Hibbit, Karlsson & Sorensen, 1996.